



OPEN Parametric design and multiple objective intelligent optimization of marine nuclear turbine aerothermodynamics under variable conditions

Lei Zhang✉, Guobing Chen, Yu-Ang Shi✉ & LuoTao Xie

Our goal is to improve the aerothermodynamics performance of the marine nuclear-powered turbine and control the exhaust humidity of the blade grid, thereby improving the operating efficiency and power of the turbine and ensuring safety. We propose a method for parameterized reconstruction of steam turbine blade profiles based on their geometric parameters using a coordinate equation developed based on the third-order Bezier curve. By combining the blade parameterized reconstruction method with a Kriging approximation model and a multi-objective genetic algorithm (GA), we developed an optimized system for thermodynamic performance in turbines. The optimization objective was the cascade core thermal parameters of steam turbine under multiple operating conditions. The design parameters were the geometric parameters of the parameterized blade profile. Based on the calculation results of wet steam non-equilibrium condensation flow of steam turbine, the optimization method and process of multi-objective thermodynamic performance of steam turbine blades based on Kriging model were proposed. Then, we executed parameterized reconstruction of a Dykas planar cascade and a steam turbine 3D cascade to achieve multi-parameter, multi-condition design optimization of planar and 3D cascades. The analysis results showed that after optimizing the turbine cascade under different operating conditions, the outlet humidity decreased by 6.1–8.9%, the maximum droplet diameter decreased by 11.4–15.8%, and the isentropic efficiency increased by 0.6–0.9%. Using the proposed novel method, the isentropic efficiency and stage power of steam turbine cascades at variable operating conditions were enhanced, thermodynamic parameters (e.g., velocity, temperature, and pressure) were more homogeneously distributed, and overload condition sites showed more significant improvements. Thus, the proposed method achieved multi-condition, multi-constraint thermodynamic performance design optimization of wet steam turbine blades, thereby providing insights for intelligent design optimization and operation of wet steam turbine cascades.

Keywords Turbine, Thermodynamic performance, Parameterized reconstruction, Wet steam, Design optimization, Variable conditions

List of symbols

CFD	Computational fluid dynamics
GA	Genetic algorithm
LHS	Latin hypercube sampling
RMDD	Reduction in maximum droplet diameter
NSGA	Nondominated sorting genetic algorithm
B	Blade width
γ	Mounting angle
β_1	Geometric inlet angle
β_2	Geometric outlet angle

Power Engineering College, Naval University of Engineering, WuHan 430033, People's Republic of China. ✉email: lzhang_magic@163.com; 15202742107@163.com

r_1	Leading-edge arc radius
r_2	Trailing-edge arc radius
φ_1	Leading-edge wedge angle
φ_2	Trailing-edge wedge angle
h_1	Bezier curve control variables
h_2	Bezier curve control variables
Y_1	Grating outlet humidity at the rated conditions
Y_2	Grating outlet humidity at high flow conditions
η_{s0}	Isentropic efficiency of the prototype blades
η_{s1}	Isentropic efficiency at rated conditions
η_{s2}	Isentropic efficiency at high flow conditions

Nuclear-powered steam turbines play a very significant role as the main power equipment of nuclear-powered ships, floating nuclear power plants, nuclear-powered icebreakers and other offshore platforms. Nuclear wet steam turbines for ships have complex operating conditions and high mobility requirements. High-power single-cylinder steam turbine blades are subjected to high-humidity steam and complex stress. High steam humidity can cause low output power, low efficiency, and long-term blade erosion in steam turbines, making the blade prone to damages or fractures, thus jeopardizing the safety of steam turbines. Thus, the thermodynamic performance of steam turbines under different conditions should be considered, and the humidity of the last few stages should be strictly controlled during the design of nuclear-powered steam turbines^{1,2}.

The optimization design of turbine blades is crucial for the economy, reliability, and safety of turbine equipment. The contemporary methods used for design optimization of turbomachines such as steam turbines use the geometric parameterized modeling of blades. Li et al.³ carried out parameterized modeling of steam turbine blades. They considered three characteristic sections along the height of static blades and four characteristic sections along the height of moving blades and adopted the non-uniform B-spline function to fit the blade profile for each 2D characteristic section. Miao et al.⁴ used the non-uniform B-spline curve method to parameterize the blade profiles of a hydraulic turbine by inverting the control points of the non-uniform B-spline curve using data points on the blade profile. Bastl et al.⁵ achieved multi-plane parameterization of turbine blade cascades using the B-spline curve method, achieving improved efficiency and effectiveness of turbine blade design optimization. Mehrdada et al.⁶ proposed the continuous-curvature parameterization method considering blade profiles with 33 geometric parameters and obtained an efficient blade structure through parameter optimization. Moradtabrizi et al.⁷ optimized the geometrical shapes of wind turbine blades using the Bezier curve to determine the geometrical shapes of the blades, with the control point of the Bezier curve as the design optimization variable. Gribin et al.⁸ reconstructed turbine blades with 13 parameters that were closely related to the thermodynamic and strength performance of the blades based on the Bezier curve. To construct an optimal blade profile, the Bezier curve parameters as well as the key blade profile parameters must be considered. The performance of the above methods has been evaluated based on their ability to represent a diverse range of blade profiles while minimizing the number of control points. In this study, the Bezier curve had fewer control points, making it suitable for curved surface peaks and concave curves; it also offers precise control over the curve shape. It also accurately reconstructed the blade profile by combining key geometric parameters and is easily programmable.

Thermodynamic numerical optimization methods that combine computational fluid dynamics (CFD) and intelligent optimization algorithms have rapidly developed in the field of thermodynamic design optimization⁹, especially for multi-objective design optimization. Typical optimization algorithms include GAs, ant colony optimization algorithms, and particle swarm optimization algorithms^{10,11}. GA has high parallelism, good global convergence, high robustness, and does not require a specific objective function gradient; thus, it has been widely used for the design optimization of turbomachinery. Trigg et al.¹² used GAs for the thermodynamic design of the 2D profile of a steam turbine blade; they considered profile loss under a given condition as the objective function. Dennis et al.¹³ used total pressure loss as the objective function, handled constraints using the quadratic sequence programming method, and used a robust GA to optimize the design of a linear profile cascade. Adjei et al.¹⁴ used the B-spline curve to parameterize a turbine blade and used the combination of a GA and a response surface method to optimize performance parameters such as blade total pressure loss and outlet vortex angle, obtaining smooth blade profiles. Couto et al.¹⁵ achieved multi-objective performance optimization of a turbine blade by considering the turbine blade mass, natural frequency, and vibration displacement as the objective function; the blade material and structural parameters were the design parameters, and they combined the method with GA. Zhang et al.¹⁶ introduced the NSGA-II algorithm to achieve the multi-objective optimization of turbine cascade flow channels by considering the thermodynamic performance and erosion resistance of a high-pressure turbine.

Randomized algorithms such as GA require hundreds of iteration cycles for optimization, and each iteration comprised a fluid performance calculation or a finite element analysis of structural strength. For large turbomachines, one simulation might take several hours or even days. For multidisciplinary design optimization, multi-objective design optimization, or multi-condition design optimization issues, optimization algorithms are often used in combination with experimental design and surrogate modeling methods. The surrogate modeling method is used to construct objective functions with design parameters as variables, which matches the actual simulation results with the given sample points and response values. In an iterative optimization process, the model is continuously updated, which improves the model accuracy and accelerates the iterative convergence.

Several surrogate modeling methods have been developed, namely, polynomial response surface¹⁷, radial basis function¹⁸, and Kriging model^{19,20}. Huang et al.²¹ optimized the shape of an aero-engine turbine disc under thermal and mechanical loads based on the Kriging model. Bakhtiari²² redesigned the stator of a transonic

compressor test bed using 75 design parameters and two objective functions, proposed a multi-objective optimization procedure based on artificial neural networks (ANNs), and used a combination of a Kriging model and a GA to optimize the stator. To decrease the steam turbine thermodynamic losses of power plants, Kadhimi et al.²³ established a Kriging model to predict the total stage pressure loss coefficient, realizing an iterative design for representing steam turbine performance. Chen et al.²⁴ used a Kriging model to predict wind turbine power performance, achieving higher prediction efficiency and stability than an ANN model. They also used a moderate and robust sampling strategy, which was essential for improving the prediction performance of the Kriging model. Cardoso et al.²⁵ demonstrated that Kriging outperformed polynomial models and closely matched Extreme Learning Machine (ELM) accuracy with moderate training data. Esfahanian et al.²⁶ optimized gas turbines via a CNN surrogate, yet its dependency on large datasets contrasted with Kriging's data efficiency. For wind energy, Wang et al.²⁷ integrated Kriging with adaptive CFD sampling to maximize wind farm AEP, reducing computational costs by avoiding excessive wake simulations. These studies highlight Kriging's superiority in balancing accuracy and efficiency for nonlinear aerodynamics, while enabling uncertainty-aware optimization—advantages critical for robust blade and turbine design.

Most contemporary studies on turbomachinery design optimization focus on single-objective or multi-objective design optimization of performance under given conditions; however, no studies have reported thermodynamic design optimization under varying conditions. Most studies have considered entropy, supercooling degree, and humidity, while few studies have considered other thermodynamic parameters of non-equilibrium condensation flows as optimization objectives. In this study, we constructed a cascade performance prediction model based on the blade profile parameterized reconstruction method and a Kriging model to study the multi-condition design optimization method of wet steam turbine blades. The optimization objectives were thermodynamic parameters under wet steam condensation flow of a nuclear steam turbine under varying conditions. We aimed to mitigate the condensation nucleation phenomenon, decrease steam humidity in the through-flow part, and account for the performance requirements of multiple condition sites, improving the multi-condition operation efficiency and safety of steam turbines.

The structure of the paper is arranged as follows: Section "Methods for parameterized reconstruction of steam turbine blade profiles" introduces the parametric reconstruction method for steam turbine blade profiles. Section "Multi-condition cascade design optimization based on CFD-based non-equilibrium condensation flow" presents the multi-condition optimization design methodology and workflow for steam turbine cascades. Section "Multi-condition moisture-removal design optimization of Dykas steam turbine cascade" describes the multi-condition dehumidification optimization design and experimental validation for the Dykas linear cascade. Section "Multi-condition, multi-objective optimization of wet steam turbine" demonstrates the application and verification of multi-objective optimization under multi-condition for a wet-steam turbine.

Methods for parameterized reconstruction of steam turbine blade profiles

The geometrical shapes of steam turbine blades, such as trailing edge, hub, and blade profile, significantly impact the distribution of thermodynamic parameters such as medium entropy, supercooling degree, and humidity as well as the distribution of condensation parameters under the condensation flow of cascade flow channels. Blade profile design optimization considerably influences the distribution of expansion rate of a steam turbine through-flow part, thus indirectly controlling the condensation process, increasing stage efficiency and power, and decreasing humidity. The profile of a steam turbine blade includes four curves, namely, a leading-edge circular arc curve DE, a trailing-edge circular arc curve GH, a suction-edge curve GD, and a pressure-edge curve HE (Fig. 1). We used the third-order Bezier curve to describe the coordinate equations of the pressure-edge curve HE and the suction-edge curve GD and the circle curve equation to represent the leading-edge circular arc curve DE and the trailing-edge circular arc curve GH. Thus, we obtained the coordinate equations of the four

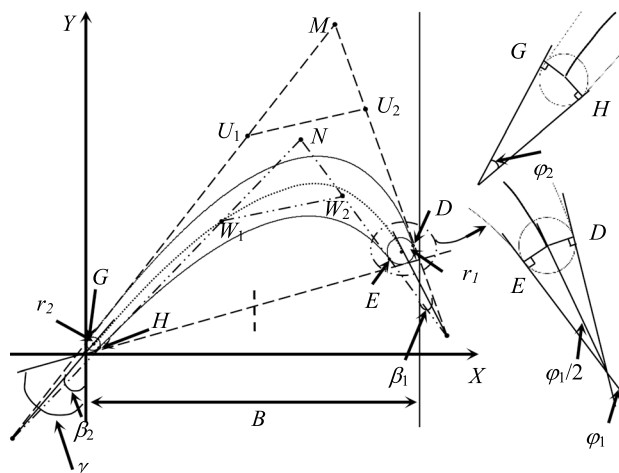


Fig. 1. Parametrization of blade profile.

curves. As shown in Fig. 1, U_1 , U_2 , W_1 , and W_2 denote the points dividing the lines GM, MD, HN, and NE in a certain proportion (specifically, h_i , $0 \leq h_i \leq 1$). For example, h_1 indicates the length ratio of line MU_1 to line MG.

The pressure-edge curve HE was described by a third-order Bezier curve with polygonal control vertices H , W_1 , W_2 , and E . Its coordinate parameter equation is shown in Eq. (1):

$$\begin{cases} x_{\text{PRE}}(t) = x_H(1-t)^3 + x_{W_1}3(1-t)^2t + x_{W_2}3(1-t)t^2 + x_Et^3 \\ y_{\text{PRE}}(t) = y_H(1-t)^3 + y_{W_1}3(1-t)^2t + y_{W_2}3(1-t)t^2 + y_Et^3 \end{cases} \quad (1)$$

The suction-edge curve GD was described by a third-order Bezier curve with polygonal control vertices G , U_1 , U_2 , and D . Its coordinate parameter equation is shown in Eq. (2):

$$\begin{cases} x_{\text{SUC}}(t) = x_G(1-t)^3 + x_{U_1}3(1-t)^2t + x_{U_2}3(1-t)t^2 + x_Dt^3 \\ y_{\text{SUC}}(t) = y_G(1-t)^3 + y_{U_1}3(1-t)^2t + y_{U_2}3(1-t)t^2 + y_Dt^3 \end{cases} \quad (2)$$

where t is the auxiliary parameter of the coordinate parameter equation of the third-order Bezier curve, $t \in [0, 1]$, and x and y are the horizontal and vertical coordinates of the Cartesian coordinate system, respectively.

The leading-edge circular arc curve DE and the trailing-edge circular arc curve GH were expressed by the respective circular curve equations (Eqs. (3) and (4), respectively):

$$(x - x_1)^2 + (y - y_1)^2 = r_1^2 \quad (3)$$

$$(x - x_2)^2 + (y - y_2)^2 = r_2^2 \quad (4)$$

where r_1 is the leading-edge arc radius, r_2 is the trailing-edge arc radius, x_1 is the horizontal coordinate of the leading-edge arc center O_1 , x_2 is the horizontal coordinate of the trailing-edge arc center O_2 , y_1 is the vertical coordinate of the leading-edge arc center O_1 , and y_2 is the vertical coordinate of the trailing-edge arc center O_2 .

Equations (1–4) constitute the parametric equations of the blade profile. The coordinates of the polygonal control vertices H , W_1 , W_2 , E , G , U_1 , U_2 , and D describing the pressure-edge curve and the suction-edge curve as well as the coordinates of the leading-edge arc center O_1 and the trailing-edge arc center O_2 were obtained according to their geometrical relationships. By substituting the coordinates into the coordinate equations of the four curves, parameterized reconstruction of the blade profile was achieved. This process involved 12 design parameters, which included 8 geometric structural parameters (blade width B , mounting angle, leading-edge arc radius r_1 , trailing-edge arc radius r_2 , geometric inlet angle, geometric outlet angle, leading-edge wedge angle, and trailing-edge wedge angle) and 4 Bezier curve shape control parameters (h_1 , h_2 , h_3 , and h_4).

Using the blade profile parameterized reconstruction method based on the Bezier curve, we reconstructed the blade profile curve with varying mounting angles, trailing-edge radius, trailing-edge wedge angles, and trailing-edge outlet angles (Fig. 2). Thus, by adjusting any design parameters, we obtained different shapes of blade profiles, laying the foundation for the qualitative analysis of condensation flows and the design optimization of wet steam stage blades.

Multi-condition cascade design optimization based on cfd-based non-equilibrium condensation flow

In multi-condition design optimization based on the CFD non-equilibrium condensation flow analysis, the performance requirements are comprehensively considered under multiple conditions and a sample space is built by combining the Latin hypercube sampling (LHS) experimental design method²⁸. Thereafter, a cascade geometric parameter and cascade performance prediction model are established based on the Kriging model using non-equilibrium condensation numerical calculations as the sample data. We also considered the thermodynamic parameters obtained from the prediction model as the optimization objectives and used a multi-objective intelligent optimization algorithm to determine the optimal combination of blade geometric design parameters, which enabled optimization of performance under multiple conditions.

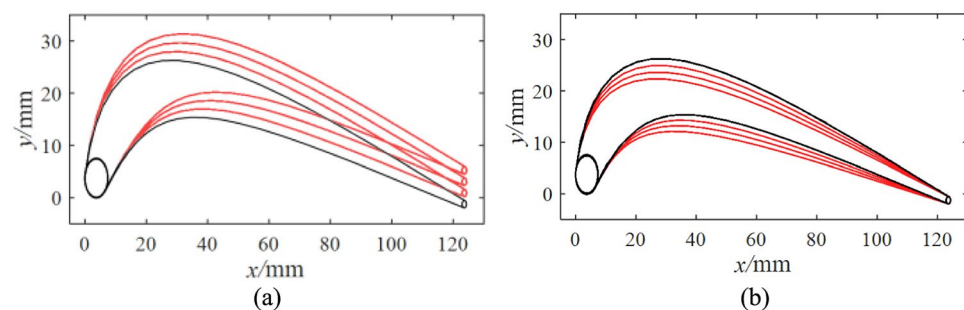


Fig. 2. Schematic diagram of blade profile curves varying with geometric parameters (the black curve represents the original blade profile, and the red curve represents the modified blade profile): (a) mounting angle from 51.44° to 56.84°, (b) geometric outlet angle from 17.04° to 21.84°.

Objective functions of multi-condition design optimization of steam turbine cascades

We parameterized a blade profile using third-order Bezier curves. There were 12 blade profile parameters, which included 8 blade profile geometric structural parameters ($B, \gamma, r_1, r_2, \beta_1, \beta_2, \varphi_1$, and φ_2) and 4 Bezier curve shape control parameters (h_1, h_2, h_3 , and h_4). The 12 parameters determined a unique blade profile, and each parameter corresponded to a design parameter of a blade profile; in the moisture-removal design optimization of steam turbine blade profile, n design parameters were selected from the 12 parameters, and the remaining $12-n$ parameters were constants; n satisfied the condition $2 \leq n \leq 12$, and two objective functions were determined using Eq. (5):

$$\text{Min}[Y_1(X_1, X_2, \dots, X_n), Y_2(X_1, X_2, \dots, X_n)] \quad (5)$$

The constraints were calculated using the following equations:

$$\begin{aligned} l_d \cdot X_1 &\leq X_1 \leq X_1 \cdot l_u \\ l_d \cdot X_2 &\leq X_2 \leq X_2 \cdot l_u \\ &\vdots \\ l_d \cdot X_n &\leq X_n \leq X_n \cdot l_u \\ \eta_{01} &\leq \eta_1, \eta_{02} \leq \eta_2 \end{aligned}$$

where X_1, X_2, \dots , and X_n are the 1st, 2nd, ..., and n th design parameters; Y_1 and Y_2 refer to the objective function under different conditions, which included performance indicators such as cascade outlet humidity, cascade efficiency, and power. For the constraints, l_d was 0.8–0.9 and l_u was 1.1–1.2, and the constraints were set according to specific parameters such as efficiency and power.

Cascade multi-objective moisture-removal optimization method based on kriging model

With the initial (before optimization) blade profile parameters as the center points and with each design parameter meeting the constraints of the multi-objective problem, the LHS experimental design method was used to build the sample matrix $X_{P \times n}$ of the blade profile design parameters. The matrix $X_{P \times n}$ consisted of n columns of design parameters and P rows of samples, and P was no less than $3n$. Each row of the sample matrix corresponded to a blade profile, indicating a total of P blade profiles. Each group of design parameters represented a blade profile. Then, cascade and flow field models were established based on the blade profiles, and a 3D flow field numerical simulation method was used to calculate the flow features of wet steam in the cascade consisting of blades. Thus, the objective function value sample matrix was obtained as $Y_{P \times 2} = [Y_1, Y_2]$, and the objective function value sample matrix Y consisted of two columns and P rows.

With the sample matrix $X_{P \times n}$ and the objective function value sample matrix $Y_{P \times 2}$ of design parameters as the basic data, a surrogate model was built for blade design parameters and objective functions based on the Kriging model⁹. The surrogate model Ψ was expressed using Eqs. (6–8):

$$\Psi = f(x_k) T \beta^* + r(x_k) T \gamma^* \quad (6)$$

$$\beta^* = (FTR - 1F) - 1FTR - 1Y \quad (7)$$

$$\gamma^* = R - 1(Y - F\beta^*) \quad (8)$$

where x_k is the design parameterization, $k = 1, 2, \dots, n$; $f(x_k)$ is the row vector of the function value $f(x_k)$ of the parameter x_k of the design parameterization, and $f(\cdot)$ is a first-order polynomial function; $r(x_k)$ is the column vector of the correlation function between the parameter x_k of the design parameterization and the samples in the sample matrix $X_{P \times n}$; the elements of the matrix F are the function value $f(x_{ik})$ ($i = 1, 2, \dots, P, k = 1, 2, \dots, n$) of each sample of the parameter x_k of the design parameterization; R is the correlation function matrix, with each element expressed as $R(X_i, X_j) = \prod_{k=1}^n \exp(-\theta_k d_k^2)$, where $l = 1, 2, \dots, P, j = 1, 2, \dots, P, k = 1, 2, \dots, n$, θ_k is the anisotropy parameter; and d_k is the distance between any two points in the sample.

Any M groups of design parameters that satisfied the multi-objective constraints were selected to build a cascade model, where $3 \leq M \leq P$. The 3D flow field numerical simulation calculation method was used to calculate the M -group objective function value matrix of the flow features of wet steam in the cascade. Meanwhile, the cascade model built on M -group design parameters was substituted into the surrogate model Ψ to calculate the objective function value matrix, and the M -group objective function value matrix of the flow features of wet steam in the cascade calculated using the 3D flow field numerical simulation calculation method was compared with that calculated using the surrogate model Ψ in a one-to-one comparison. If the surrogate model satisfied the computational accuracy requirements, the multi-objective non-dominated GA (NSGA-II)¹⁶ was used to optimize the Kriging surrogate model Ψ , until the optimal objective functions $Y_{1\text{best}}$ and $Y_{2\text{best}}$ and the corresponding optimal values of the blade profile design parameters were calculated; otherwise, the number of sample points was increased until the surrogate model satisfied the computational accuracy requirements.

Figure 3 illustrates the process of the multi-objective moisture-removal optimization method for steam turbine cascades based on the Kriging model.

Multi-condition moisture-removal design optimization of Dykas steam turbine cascade

In this section, we applied the multi-condition optimization method based on the CFD non-equilibrium condensation flow calculation method to optimize the design of a Dykas planar cascade²⁹. The optimal values of

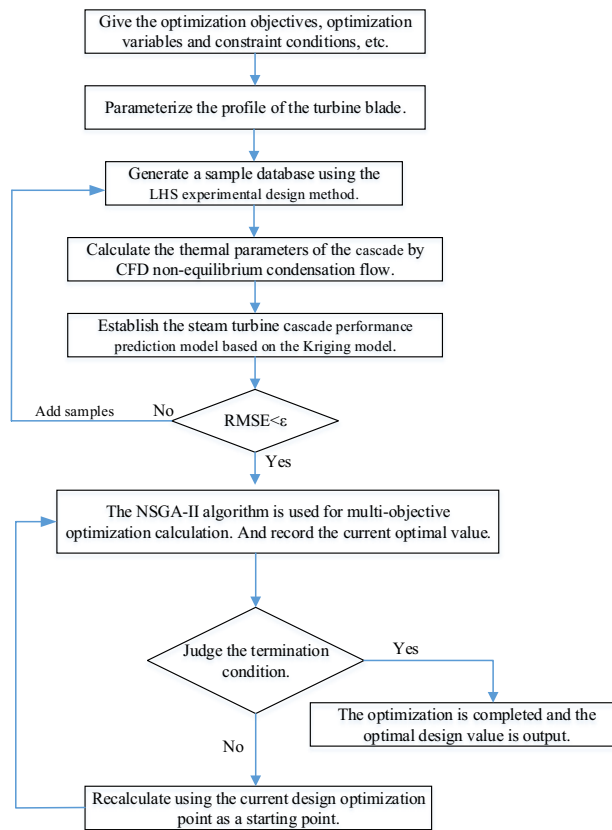


Fig. 3. Flow chart of multi-condition moisture-removal design optimization for Dykas turbine blade.

the design parameters of the Dykas planar cascade were determined under multiple constraints to minimize the wet steam loss of rated condition sites and overload condition sites of steam turbines.

Multi-objective optimization function of moisture-removal in Dykas steam turbine cascade

The blade profile curve of the Dykas steam turbine cascade consisted of four parametrized curves with eight geometric structural parameters and four Bezier curve control parameters. As indicated in reference³⁰, the wet steam non-equilibrium condensation flow affecting wet steam loss mainly occurred at the blade suction surface. Thus, structural parameters related to the pressure-surface curve (geometric outlet angle β_2 , trailing-edge wedge angle φ_1 , and Bezier curve control parameters h_3 and h_4) were considered constant. To ensure the structural strength of the optimized cascade and to prevent the cascade from becoming thin and flat during the optimization process, the leading and trailing edges of the cascade (blade width B) were fixed during design optimization, and the other seven parameters ($\gamma, \beta_1, \varphi_1, r_1, r_2$, and Bezier curve control parameters h_1, h_2) were considered as the design parameters. The values of the initial design parameters were increased by $\pm 10\%$ to obtain a range of values for the design parameters. To decrease the influence of the units of the design parameters on the results, all parameters except the Bezier curve control parameters h_1 and h_2 were normalized with the initial blade profile parameters as references. The multi-objective optimization problem was expressed using Eq. (9):

$$\begin{aligned}
 & \text{Min } [Y_1(\gamma, \beta_1, \varphi_1, r_1, r_2, h_1, h_2), Y_2(\gamma, \beta_1, \varphi_1, r_1, r_2, h_1, h_2)] \\
 & \text{s.t. } \begin{cases} 46.33 \leq \gamma \leq 56.63 & 15.17 \leq \beta_1 \leq 18.54 \\ 1.04 \leq r_1 \leq 1.27 & 9.50 \leq r_2 \leq 11.61 \\ 0 < h_1 < 1 & 0 < h_2 < 1 \\ 5.22 \leq \varphi_1 \leq 6.38 \\ \eta_{s01} \leq \eta_{s1} < 1 & \eta_{s02} \leq \eta_{s2} < 1 \end{cases} \quad (9)
 \end{aligned}$$

where Y_1 and η_{s1} are the cascade outlet humidity and isentropic efficiency at the rated condition site respectively; Y_2 and η_{s2} are the cascade outlet humidity and isentropic efficiency at the overload condition site, respectively; η_{s0} is the isentropic efficiency of the prototype cascade. During design optimization, isentropic efficiency was taken as the performance constraint, and the optimized cascade isentropic efficiency at each condition site was set to be not smaller than that of the prototype cascade. It was expressed as $\eta = (h_{in} - h_{out}) / (h_{in} - h_{out,s})$, where h_{in}

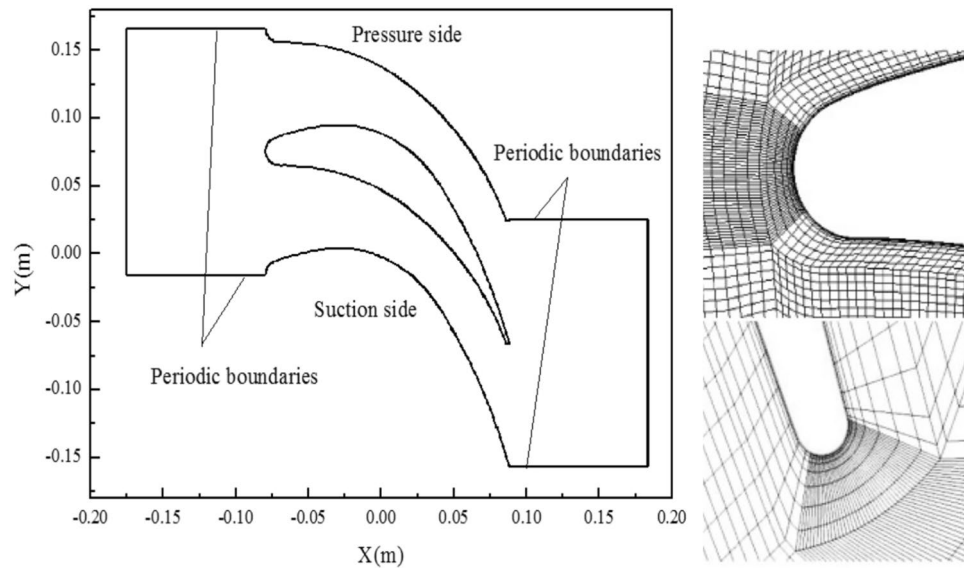


Fig. 4. The Dykas cascade channel model and the meshes near the leading edge and the trailing edge.

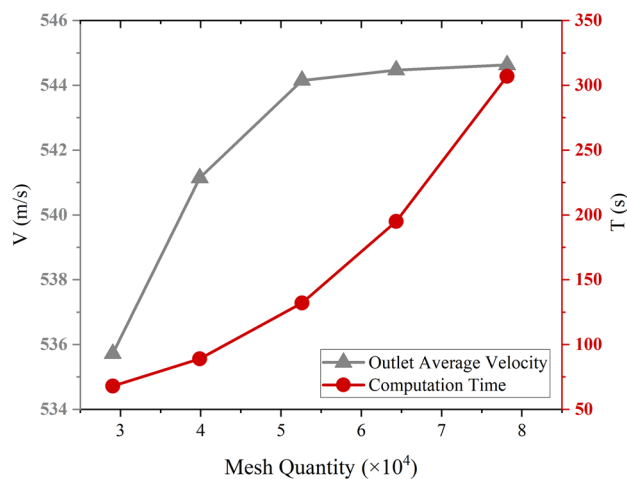


Fig. 5. The grid independence verification.

is the actual enthalpy of cascade inlet, and h_{out} is the actual enthalpy of cascade outlet, and $h_{out,s}$ is the isentropic enthalpy of outlet.

Based on the sample space generated by the blade profile parameters, the Dykas blade profile curves and cascade flow field channels were established and combined with the proposed non-equilibrium condensation flow calculation method³¹, and then, the flows of the steam turbine cascade flow channels were calculated. The Dykas cascade channel model and the meshes near the leading edge and the trailing edge are shown in Fig. 4. The grid independence verification of the computational model shows that when the mesh number increases to 52,608, there is no significant difference between the computed results but the computation time is greatly increased (see Fig. 5).

The mesh cell number is finally 52,608, We used the wet steam model IAPWS-IF97 during the calculation. The turbulence model adopted the standard SST k- ω model, the convection term adopted the upwind format, the blade surface and the rim-hub surface adopted the no-slip wall condition, the inlet/outlet boundary condition adopted the mass flow inlet and the pressure outlet, and the iterative convergence accuracy was set to 1.0×10^{-4} . According to the optimized cascade geometric parameters, a cascade channel model was established. The detailed computational and experimental boundary conditions are that the inlet total static pressure is 0.089 MPa, the total temperature is 373.15 K, and the average down-stream static pressure of the outlet is 0.039 MPa.

The non-equilibrium condensation flow calculation method was used to obtain the thermodynamic performance of the cascade under two conditions, and the calculated blade surface pressure results were compared with the experimental data from reference³¹, as shown in Fig. 6.

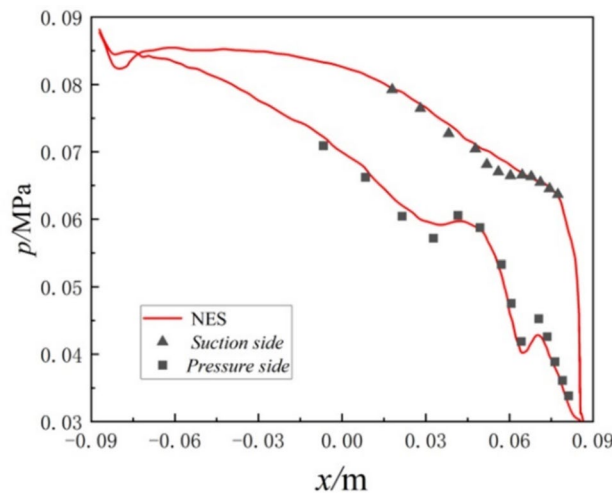


Fig. 6. Comparison of calculated and experimental values and pressure distribution on the blade surface.

The calculated and experimental values showed similar variation trends and relatively consistent pressure distributions, which indicated the high calculation accuracy of the proposed non-equilibrium condensation flow calculation method. The response values (Y_1 , η_{s1} , Y_2 , and η_{s2}) associated with the blade profile under the rated and overload conditions were obtained using the above non equilibrium condensation flow calculation method. During the design optimization of the steam turbine cascade, seven parameters were used as inputs to the Kriging model, and the humidity and isentropic efficiency under rated and overload conditions were used as outputs. The LHS design method was selected in the paper to generate sample data. This method not only has good flexibility, uniformity and operability, but also can design accurate variable dimensions and sample numbers according to actual problems. Thus, a sample database of 7 factors and 200 levels for the blade cascade geometry channel was established. Before the approximation model was constructed, the design parameters and objective functions were normalized.

After repeated iterative calculations, 200 sample data were determined. Among them, 90% of the samples were used as the training set and 10% of the samples were used as the test set. The RMSE of the training set was calculated to be 1.62% and that of the test set to be 1.83%. It can be seen that the optimization algorithm proposed in this paper has a relatively high calculation accuracy. To further analyze the influence of each structural parameter on the objective functions of humidity and efficiency, the constructed Kriging model was used to calculate the objective function values by changing one structural design parameter at a time; thus, the influences of the seven design parameters on the efficiency and humidity were obtained (Fig. 7).

As observed in Fig. 6, the influence of design parameters on the same objective function under different conditions exhibited a similar trend, but the influence of design parameters on efficiency and humidity was not the same. Under the rated condition, the suction-surface trailing-edge control parameter h_2 of the third-order Bezier curve and the trailing-edge wedge angle had a greater influence on efficiency, while the mounting angle had a greater influence on humidity; the control parameter of the third-order Bezier curve had a relatively smaller influence on humidity.

Analysis of multi-condition multi-objective optimization results for Dykas planar cascade

We performed multi-condition design optimization for the Dykas steam turbine cascade, obtaining the optimized cascade blade profile. The selection of optimization parameters for the NSGA-II algorithm in this paper refers to references^{32,33}, and considers that this study includes 2 objectives and 7 variables, which is of medium scale. It can cover the search space without a large population, and the Pareto frontiers of the 2 objective functions are relatively easy to obtain. Comprehensively considering the computing resources, the population size is determined to be 50, the maximum number of iterations is 100, and the utilization of a high crossover probability of 0.9 is conducive to the global search. The Pareto stochastic frontiers of the cascade outlet humidity under two conditions are shown in Fig. 7.

As shown in Fig. 8, the Pareto optimal solutions were relatively uniformly distributed, with a total of 40 optimal solutions; the results for humidity under the rated and overload conditions were proportional to each other in the sample space; however, the humidity under the two conditions did not always reach the minimum value at the same time. Compared with the initial design value, under the Pareto optimal solution, the humidity at the two conditions decreased slightly. According to the Pareto stochastic frontiers, the humidity under the overload condition showed a greater variation, and thus, the Pareto optimal solution obtained under the overload condition was considered as the optimal solution in this study. According to the optimized design parameters, the non-equilibrium condensation flows of the final solution were calculated for the Dykas cascade at rated and overload condition sites. The calculation results were consistent with the solution optimization results, which further verified the reliability and accuracy of the presented optimization method. This paper proposes a multi-point multi-objective optimization design method. The simulation time consumption mainly includes

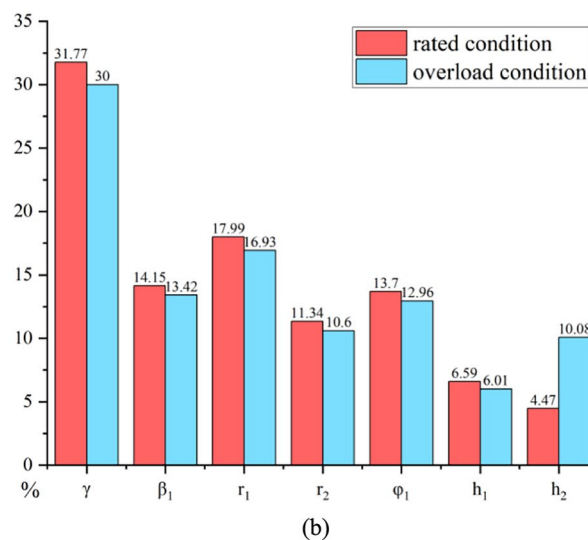
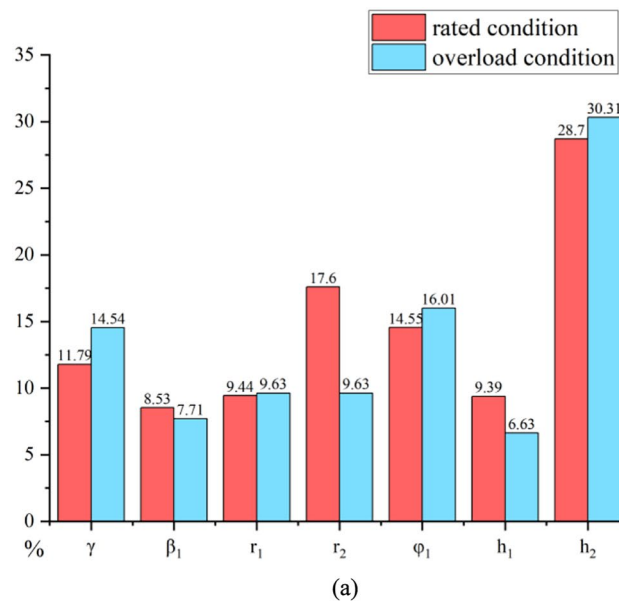


Fig. 7. Influence ratio of design parameters on objective functions under different working conditions: (a) influence of design parameters on efficiency under different working conditions, (b) influence of design parameters on humidity under different working conditions.

the time consumption of CFD calculation, the time consumption of establishing the Kriging surrogate model, and the time consumption of multi-objective optimization. When calculating the planar cascade on the 8-core i9-11900 k workstation: The CFD calculation took approximately 400 min (200 times, approximately 2 min per time), the establishment of the Kriging surrogate model took 6.7 min, and the multi-objective optimization calculation took approximately 2.6 s. It can be seen that the CFD calculation stage takes the most time. For the CFD calculation of the three-dimensional cascade of the actual steam turbine, supercomputing resources can be utilized to further improve the calculation speed.

Table 1 compares the optimized and initial results of the blade profile design parameters. Compared with the initial cascade, in the optimized blade profile, the geometrical inlet angle and the outlet control parameter h_2 of the suction-surface Bezier curve were smaller, which resulted in a smaller curvature of the suction surface of the blade profile from the throat to the trailing edge; consequently, a smoother blade suction-surface profile was obtained near the throat, along with a more uniform steam flow expansion, a lower local expansion rate, and smoother steam flow transition. Figure 9 shows the comparison of Dykas blade profile design before and after optimization.

Table 2 compares the thermal performance of the Dykas cascade before and after optimization. After optimization, under the rated condition, the outlet humidity, increase in entropy, and maximum droplet diameter

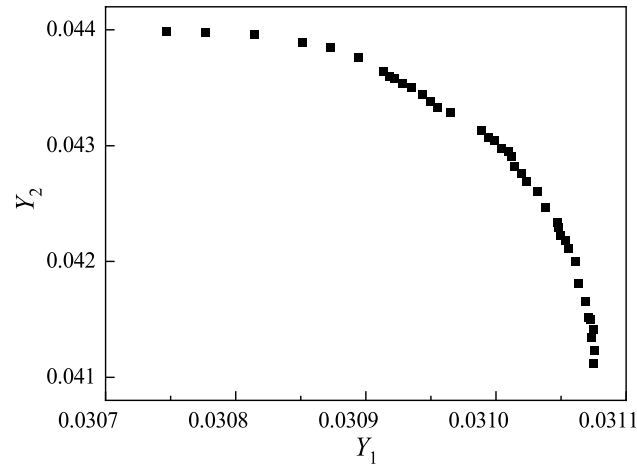


Fig. 8. Pareto stochastic frontiers of cascade outlet humidity under two conditions.

	Parameter	B/mm	$\gamma(^{\circ})$	r_1/mm	r_2/mm	$\beta_1(^{\circ})$	$\beta_2(^{\circ})$
Dykas cascade	Initial value	173.97	51.48	1.15	10.55	16.86	79.49
	Optimized value	173.97	51.44	1.30	10.60	16.02	79.49
	Parameter	$\varphi_1(^{\circ})$	$\varphi_2(^{\circ})$	h_1	h_2	h_3	h_4
Dykas cascade	Initial value	5.80	19.53	0.544	0.075	0.016	0.860
	Optimized value	6.35	19.53	0.504	0.108	0.016	0.860

Table 1. Results of multi-condition moisture-removal design optimization for Dykas turbine blade model line variables.

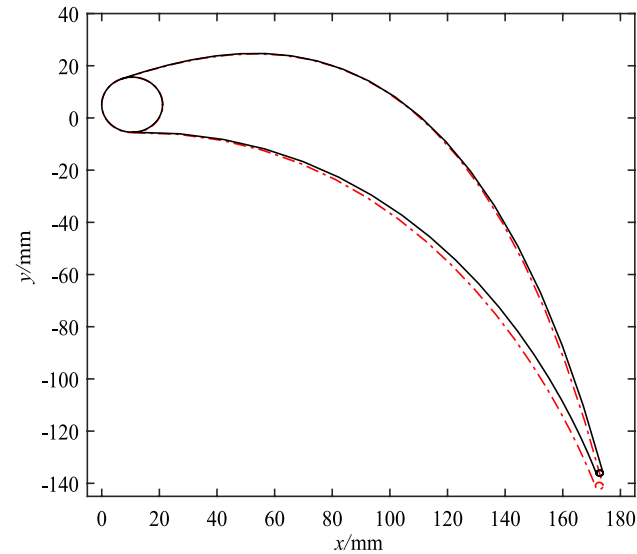


Fig. 9. Dykas blade profile before and after optimization: the solid line is the initial design, the dotted line is the optimized design.

decreased by 6.1%, 5.1%, and 11.4%, respectively, and the isentropic efficiency increased by 0.6%. Under the overload condition, the outlet humidity, increase in entropy, and maximum droplet diameter decreased by 8.9%, 15.2%, and 15.8%, respectively, and the isentropic efficiency increased by 0.9%. The smaller value of increase in entropy indicated lower thermodynamic and thermodynamic losses in the non-equilibrium condensation flow nucleation process; the smaller maximum droplet diameter indicated a decrease in erosion losses caused by wet steam.

Parameter	Increase in entropy/J/(kg k)	MDD/ μm	Isentropic efficiency/%	Maximum nucleation rate/ $1/\text{m}^3\text{s}$	outlet humidity
Before optimization (the rated condition)	25.7	0.0369	86.9	$10^{25.21}$	0.033
After optimization (the rated condition)	24.4	0.0327	87.5	$10^{25.13}$	0.031
Magnitude of change/%	-5.06	-11.38	+0.69	-16.82	-6.06
Before optimization (the overload condition)	34.3	0.0374	86.4	$10^{25.24}$	0.045
After optimization (the overload condition)	29.1	0.0315	87.2	$10^{25.15}$	0.041
Magnitude of change/%	-15.2	-15.77	+0.93	-18.72	-8.89

Table 2. Results of multi-condition moisture-removal design optimization for Dykas turbine blade.

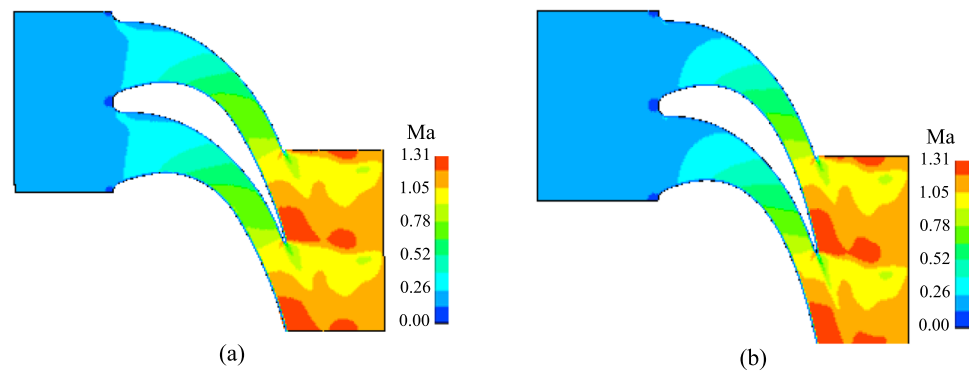


Fig. 10. Contours of Mach number for optimization and initial blade cascade under the rated condition: (a) initial and (b) optimized blade profiles.

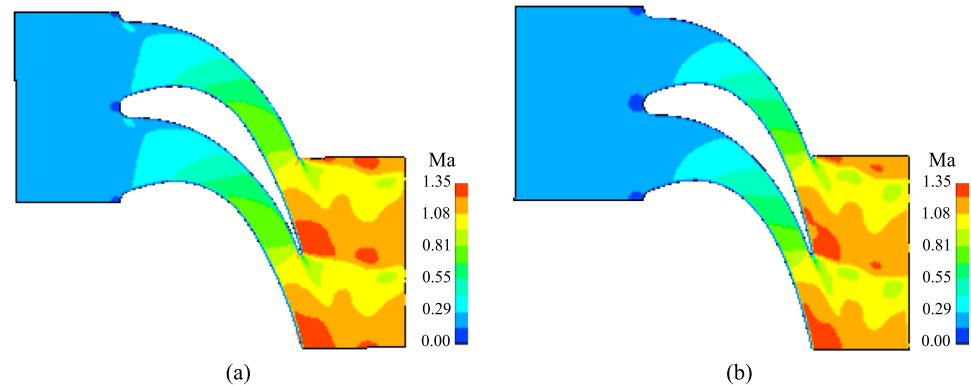


Fig. 11. Contours of Mach number for optimization and initial blade cascade under the overload condition: (a) initial and (b) optimized blade profiles.

To more intuitively analyze the non-equilibrium condensation flow features of the steam turbine cascade and the influence of blade optimization on wet steam parameters, the contours of the Mach number under rated and overload conditions before and after optimization were provided (Figs. 10 and 11). Dovetail-type condensation shock waves caused by spontaneous condensation and trailing flow impacts were observed at the trailing edge of the cascade under all conditions; the Mach number under the overload condition was greater than that under the rated condition. The optimized cascade also had a smaller Mach number and shock wave strength than the initial cascade under both conditions.

Figures 12 and 13 show the contours of the nucleation rate before and after optimization, respectively, under rated and overload conditions. The initial nucleation position was in the throat region of the trailing edge of the cascade, which did not change with the design modification; however, the nucleation rate decreased slightly, and the optimized blade profile nucleation rate nearly plateaued. Figures 14 and 15 show the contours of humidity before and after optimization, respectively, under all conditions. The optimized cascade inhibited the non-equilibrium condensation flow process and decreased steam humidity in the cascade channels under both conditions.

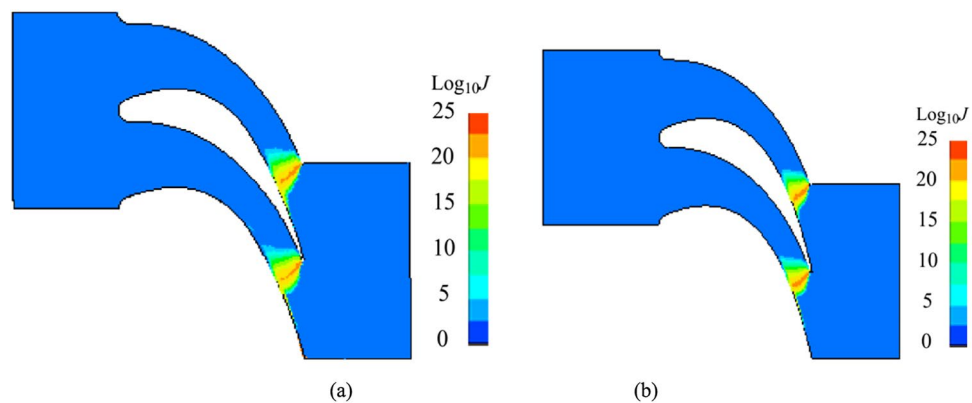


Fig. 12. Contours of nucleation rate r for optimization and initial blade cascade under the rated condition: (a) initial and (b) optimized blade profiles.

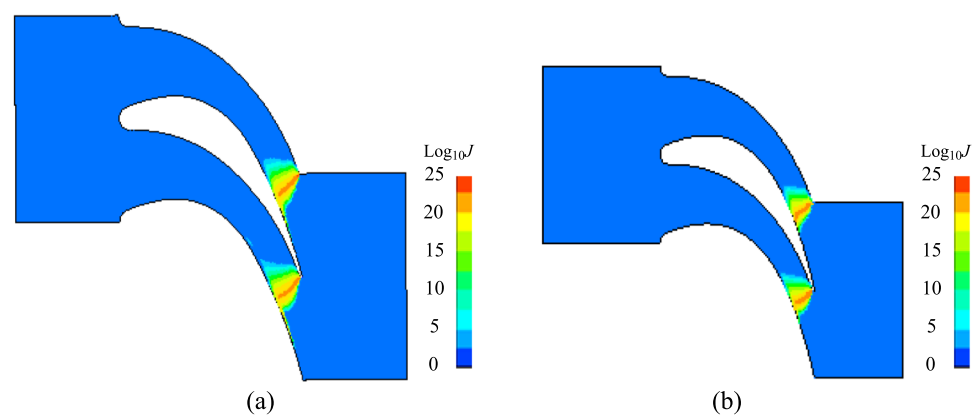


Fig. 13. Contours of nucleation rate for optimization and initial blade cascade under the overload condition: (a) initial and (b) optimized blade profiles.

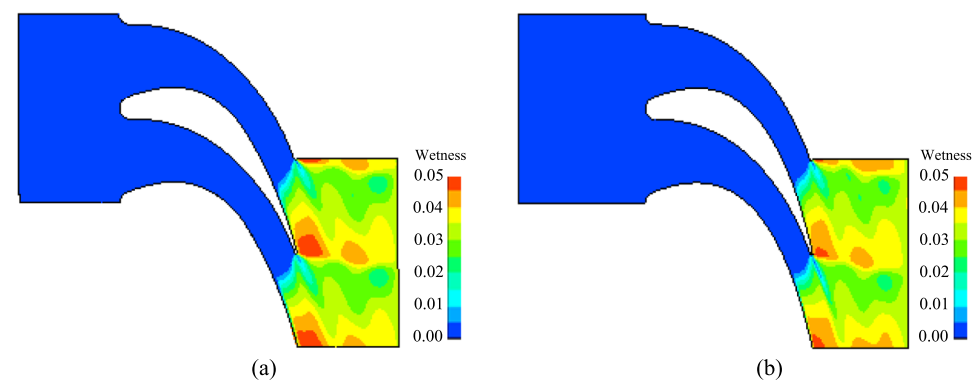


Fig. 14. Contours of humidity for optimization and initial blade cascade under the rated condition: (a) initial and (b) optimized blade profiles.

Multi-condition, multi-objective optimization of wet steam turbine

Herein, we considered a high-power-density wet steam turbine with all stages operating in the wet steam zone as the study object; two condition sites characterized by high exhaust humidity, namely, the rated and overload condition sites, were selected. The moving and static blades of the last stage of the turbine comprised multiple sections. If the proposed steam turbine blade parameterized reconstruction method was used separately for each section, there would be too many variables. Therefore, the two sections of the last-stage blade root and blade

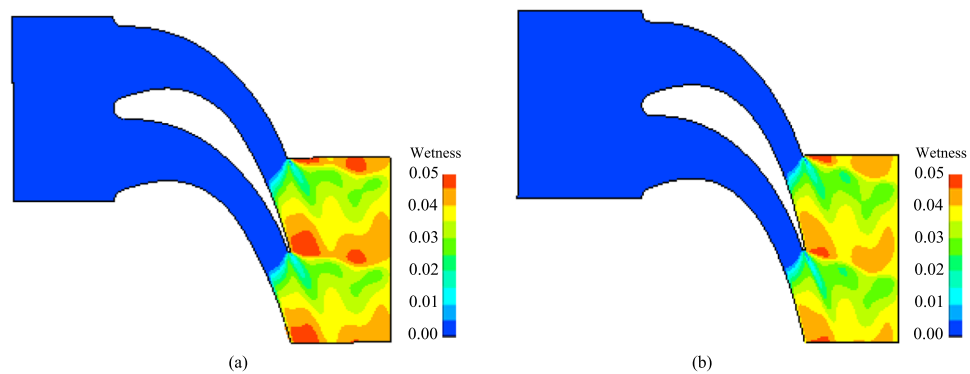


Fig. 15. Contours of humidity for optimization and initial blade cascade under the overload condition: (a) initial and (b) optimized blade profile.

top were selected as the objects for design optimization; for other sections, we considered the original design parameters. For each section, the geometrical inlet angle, geometric outlet angle, leading-edge wedge angle, leading-edge wedge angle, and mounting angle were used as the design optimization parameters. The aim of design optimization was to minimize the last-stage outlet humidity at the rated and overload condition sites considering the performance constraints of no decrease in stage efficiency and no change in stage flow at both condition sites.

The variation range of each structural parameter constraint during the optimization design and analysis of the steam turbine stage is:

$$s.t. \begin{cases} 0.9\beta_1 \leq \beta_1 \leq 1.1\beta_1 & 0.9\varphi_1 \leq \varphi_1 \leq 1.1\varphi_1 \\ 0.9\beta_2 \leq \beta_2 \leq 1.1\beta_2 & 0.9\varphi_2 \leq \varphi_2 \leq 1.1\varphi_2 \\ 0.9\gamma \leq \gamma \leq 1.1\gamma & \\ 0.99G_{01} \leq G_1 \leq 1.01G_{01} & 0.99G_{02} \leq G_2 \leq 1.01G_{02} \\ \eta_{01} \leq \eta_1 \leq \eta_2 & \eta_{02} \leq \eta_2 \leq \eta_2 \end{cases}$$

The calculation formula for the stage efficiency is as follows.

$$\eta = \frac{M_d \cdot \omega}{D(H_0 - H_{2s})} \times 100\% \quad (10)$$

D represents mass flow rate. H_0 and H_{2s} respectively represent the inlet stagnation enthalpy and the outlet static enthalpy values. The output power of the stage is equal to the product of the principal torque M_d of the moving blade and the angular velocity ω . The design parameters and optimization objectives were normalized.

To obtain enough sample data to train the Kriging model, a large number of numerical calculations of non-equilibrium condensation flows were required; it is challenging for conventional servers to meet these calculation requirements. Thus, we used a 400-core supercomputer to carry out the non-equilibrium condensation flow calculations and the multi-objective iterative optimization calculations.

Figure 16 compares the initial and optimized static blade profiles of the wet steam turbine. Based on the optimized blade structural parameters, a parameterized blade and single-channel flow field model were established. The non-equilibrium condensation flows were numerically simulated; the obtained efficiencies under the rated and overload conditions were 67.1% and 65.7%, with deviations of 0.75% and 0.48%, respectively, from those predicted by the approximation model (Fig. 17).

The cascade flow path is set as a structured grid with axisymmetric single flow path, and the grid at the blade wall, front and rear trailing edges is encrypted to ensure that the Y^+ value near the wall is controlled near 10. The grid independence test confirms that the number of grids in the cascade channel is 498,620. The non-equilibrium condensation flow calculation method in Section "Multi-objective optimization function of moisture-removal in Dykas steam turbine cascade" was used to calculate the flow field based on CFX software, and the wet steam physical property model was calculated using IAPWS-IF97 model. The interface of dynamic and static cascades is modeled using a Frozen Rotor model. The turbulence model adopts the standard SST $k-\omega$ model, the convection term adopts second-order upwind format, the standard wall function is adopted in the near wall region, and the non-slip wall condition is applied to the blade surface and rim hub surface. The iterative convergence accuracy is set to be 1.0×10^{-4} . The inlet and outlet boundary conditions are set to pressure temperature inlet and static pressure outlet. Figures 18 and 19 show the velocity distributions of 10%, 50%, and 90% blade height sections in the last-stage blade profile flows before and after optimization under the rated condition and overload conditions, respectively. Under both conditions, the flow velocity distributions before and after optimization were similar, and the velocity under the overload condition was slightly higher than that under the rated condition; after design optimization, the maximum steam flow velocities under the rated and overload conditions decreased by 4.5% and 3.3%, respectively, and the velocity distribution was more homogeneous.

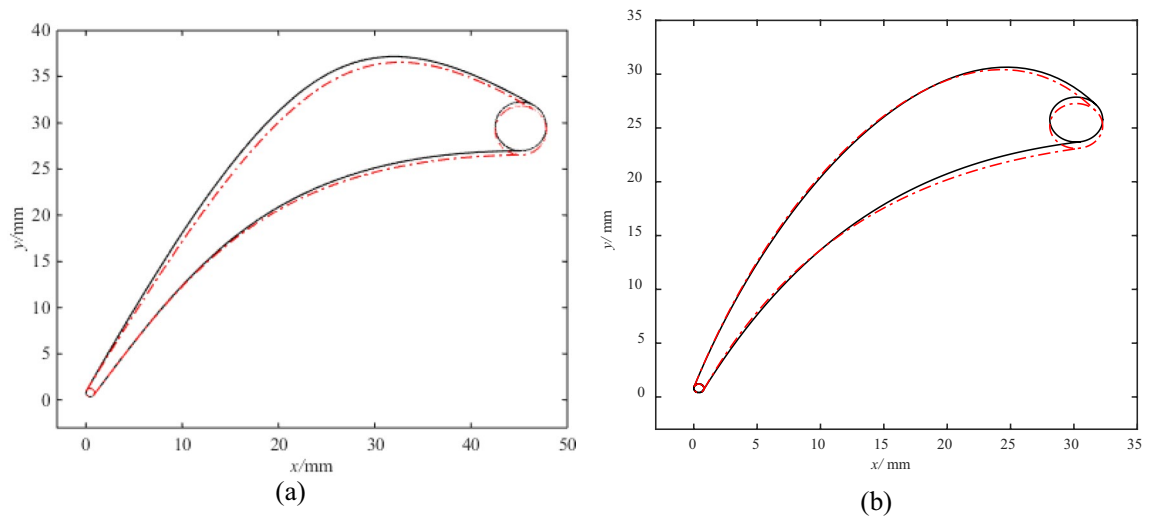


Fig. 16. Static blade profile before and after optimization: (a) blade root profile; (b) blade top profile: the solid line is the initial design; the dotted line is the optimized design.

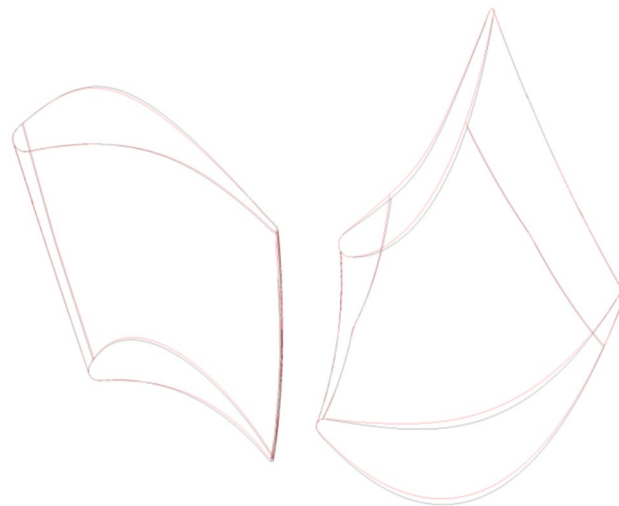


Fig. 17. 3D model before and after optimization: the black line is the initial design; the red line is the optimized design.

The cascade flow path is set as a structured grid with axisymmetric single flow path, and the grid at the blade wall, front and rear trailing edges is encrypted to ensure that the Y^+ value near the wall is controlled near 10. The grid independence test confirms that the number of grids in the cascade channel is 498,620. The non-equilibrium condensation flow calculation method in Section "[Multi-objective optimization function of moisture-removal in Dykas steam turbine cascade](#)" was used to calculate the flow field based on CFX software, and the wet steam physical property model was calculated using IAPWS-IF97 model. The interface of dynamic and static cascades is treated by a Frozen Rotor model. The turbulence model adopts the standard SST $k-\omega$ model, the convection term adopts second-order upwind format, the standard wall function is adopted in the near wall region, and the non-slip wall condition is applied to the blade surface and rim hub surface. The iterative convergence accuracy is set to be 1.0×10^{-4} . The inlet and outlet boundary conditions are set to pressure temperature inlet and static pressure outlet. Figures 16 and 17 show the velocity distributions of 10%, 50%, and 90% blade height sections in the last-stage blade profile flows before and after optimization under the rated condition and overload conditions, respectively. Under both conditions, the flow velocity distributions before and after optimization were similar, and the velocity under the overload condition was slightly higher than that under the rated condition; after design optimization, the maximum steam flow velocities under the rated and overload conditions decreased by 4.5% and 3.3%, respectively, and the velocity distribution was more homogeneous.

Figures 20 and 21 show the pressure distributions of 10%, 50%, and 90% blade height sections in the last-stage blade profile flows before and after optimization under the rated and overload conditions, respectively. The steam pressure distribution of each section of the optimized flow was more uniform after the optimization,

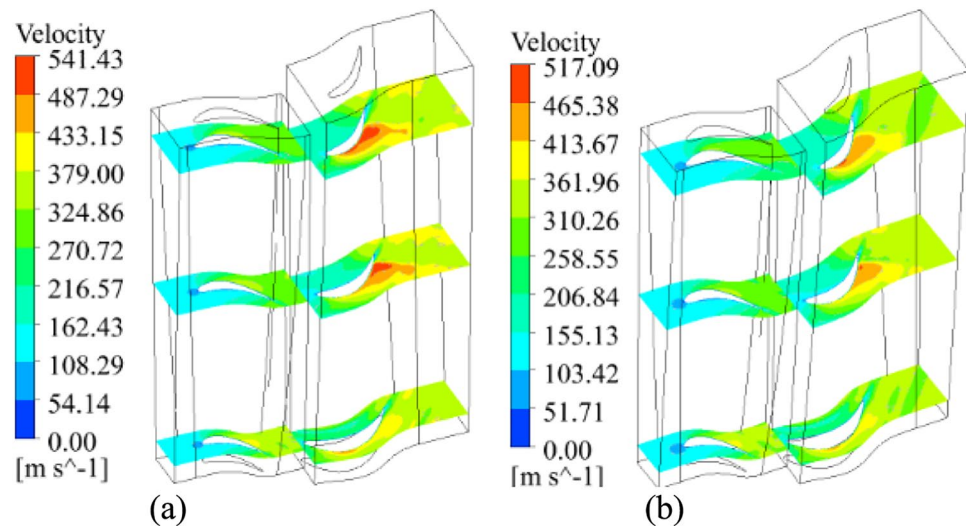


Fig. 18. Flow velocity before and after flow field optimization under the rated condition: (a) initial and (b) optimized designs.

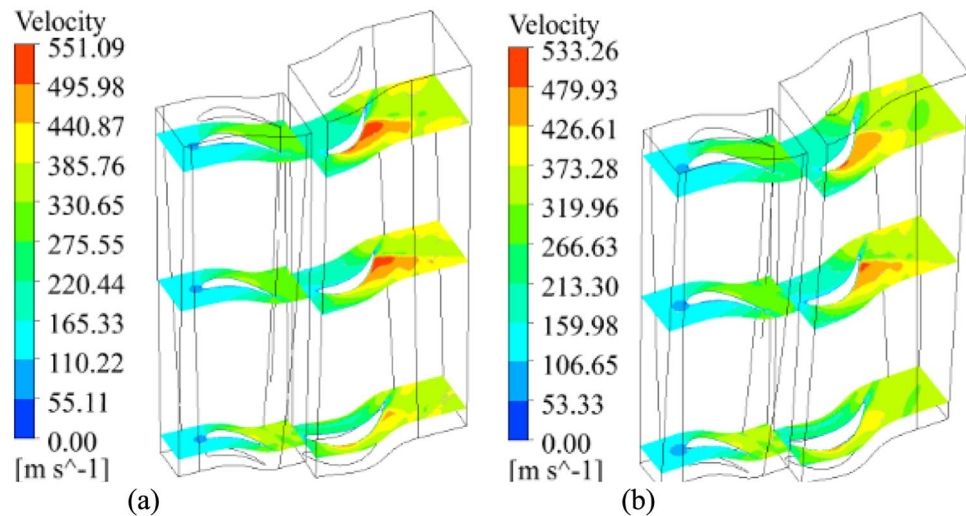


Fig. 19. Flow velocity before and after flow field optimization under the overload condition: (a) initial and (b) optimized designs.

and the area of separated flows near the trailing edge of the suction surface of the moving blade under both conditions was significantly smaller than that of the initial cascade.

Figures 22 and 23 show the humidity distributions of 10%, 50%, and 90% blade height sections in the last-stage blade profile flows before and after optimization under the rated and overload conditions, respectively. Table 3 compares the optimization results of blade multi-condition moisture-removal design for wet steam turbines under both conditions. The maximum humidity of the optimized blade profile was smaller than that of the initial blade profile, and the last-stage outlet humidity decreased from 9.41% and 9.67% to 9.36% and 9.63%, respectively, under the two conditions. After optimization, the dryness is increased by 0.5% and 0.4%, and the last-stage stage efficiency under the rated and overload conditions was 67.1% and 65.7%, which was 0.9% and 0.7% higher than that before optimization, respectively. The flow under each condition was unchanged, and the stage power increased by 0.18% and 0.19% respectively. Hence, the proposed method realized balanced performance at the overload and rated condition sites in the multi-condition optimization process.

Conclusions

In this study, we developed a third-order Bezier curve model based on the blade profile geometric parameters, enabling parameterized reconstruction of the steam turbine cascade profile; different shapes of blade profile curves were rapidly regenerated by adjusting any design parameters. Combined with 3D modeling software, a general parameterized modeling method was formed, facilitating parameterized physical modeling of the

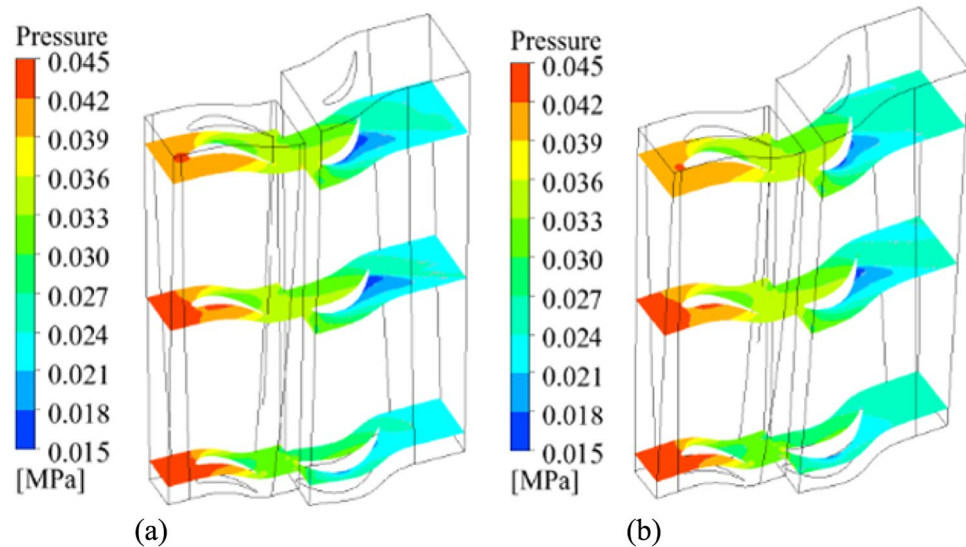


Fig. 20. Pressure distribution before and after design optimization under the rated condition: (a) initial and (b) optimized designs.

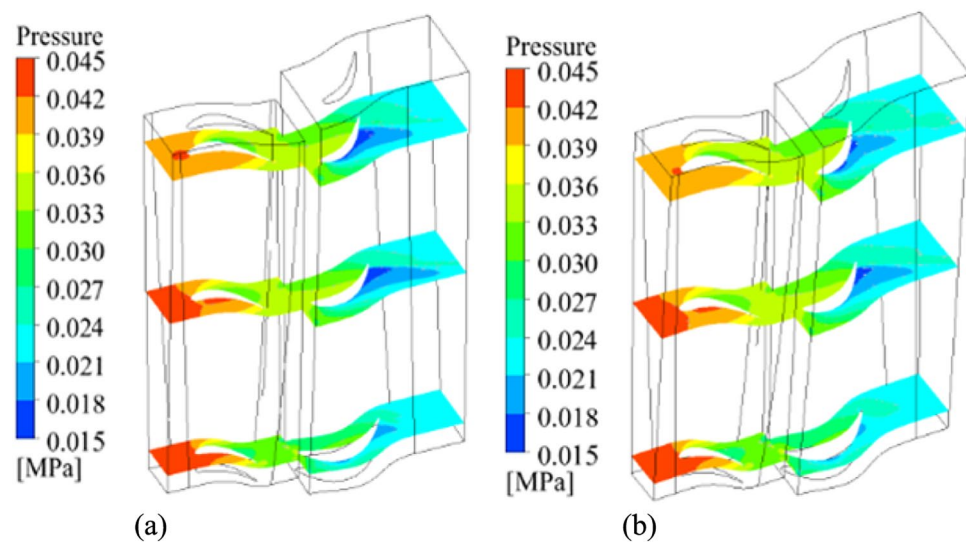


Fig. 21. Pressure distribution before and after design optimization under the overload condition: (a) initial and (b) optimized designs.

cascade and flow field. The developed parameterization model reconstruction method was easy to use and enabled accurate shape control, providing robust support for the design optimization of steam turbine blade parameters.

The CFD-based non-equilibrium condensation flow calculation method for multi-condition cascade design optimization considered the coupled objectives of cascade performance under different conditions, adopted geometric parameters that allowed accurate control of blade shape according to the design parameters, thus achieving comprehensive multi-objective performance optimization for blade profiles under diverse performance constraints. The proposed optimization method was used to investigate the individual influence of 12 blade profile geometric parameters, such as the inlet and outlet angles and Bezier curve outlet control parameter on cascade efficiency, power, humidity, along with other macroscopic performance indicators, and it also helped investigate the influence of intra-blade microscopic performance indicators such as the steam expansion rate, droplet diameter, and nucleation rate.

The proposed design optimization method was found to be suitable for the design optimization of wet steam turbine in-line and twisted blades. By optimizing blade profiles at different positions vertically along the blades, a 3D blade with excellent performance was constructed, and multi-condition moisture-removal design optimization was achieved for static and moving blade cascades in the steam turbine. This method can easily

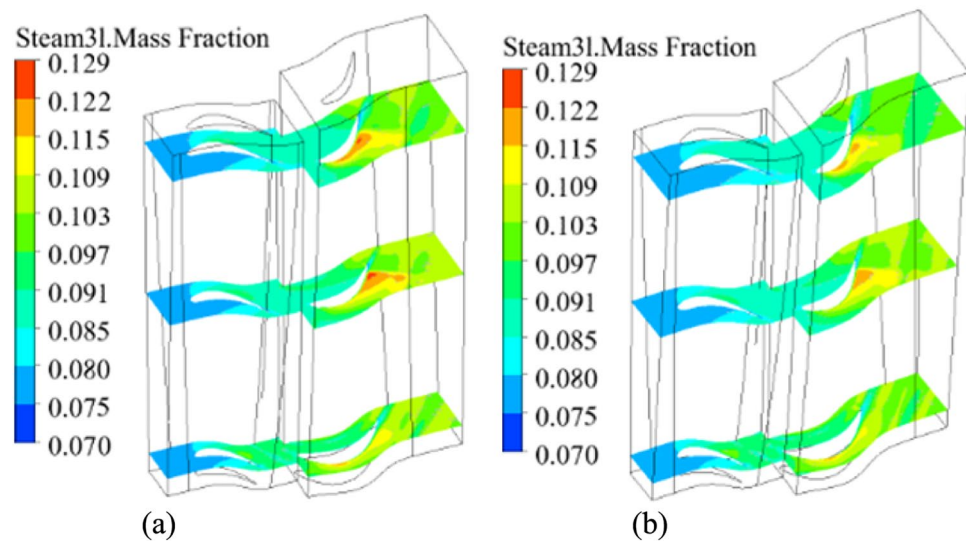


Fig. 22. Humidity distribution before and after design optimization under the rated condition: (a) initial and (b) optimized designs.

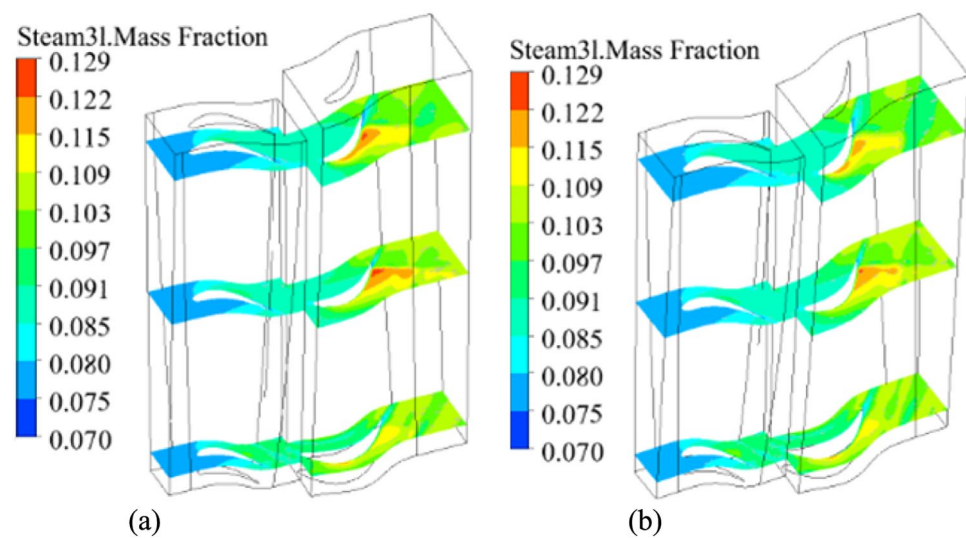


Fig. 23. Humidity distribution before and after design optimization under overload condition: (a) initial and (b) optimized designs.

Parameter	Mass flow	Stage efficiency %	Power	Outlet humidity
Before optimization (the rated condition)	1	66.5	1	0.0941
After optimization (the rated condition)	1.0001	67.1	1.0018	0.0936
Magnitude of change/%	+0.01	+0.90	+0.18	−0.53
Before optimization (the overload condition)	1	65.2	1	0.0967
After optimization (the overload condition)	1.0001	65.7	1.0019	0.0963
Magnitude of change/%	+0.01	+0.74	+0.19	−0.41

Table 3. Results of multi-condition moisture-removal design optimization for wet steam turbine blade.

realize the optimization of steam turbine power, efficiency, humidity, and other comprehensive performance and structural features by changing the optimization objectives, constraints, and design parameters, and it also provides technical support for the intelligent design optimization of wet steam turbine through-flow blades under varying conditions, suggesting broad application prospects.

Data availability

All data generated or analysed during this study are included in this published article.

Received: 16 March 2025; Accepted: 27 May 2025

Published online: 10 July 2025

References

- Kulkowski, K. et al. Nuclear power plant steam turbine-modeling for model based control purposes. *Appl. Math. Model.* **48**, 491–515 (2017).
- Sun, X. Y., Song, F. & Yuan, J. Q. Online estimation approach of the steam specific enthalpy for wet steam turbines in nuclear power plants. *Appl. Therm. Eng.* **229**, 1–11 (2023).
- Li, B. et al. Multi-disciplinary and multi-objective optimization design of long blade turbine stage. *J. Xi'an Jiaotong Univ.* **48**(1), 1–6 (2014).
- Miao, S. C. et al. Blade pattern optimization of the hydraulic turbine based on neural network and genetic algorithm. *J. Aerospace Power* **30**(8), 1918–1925 (2015).
- Bastl, B. & Michálková, K. Automatic generators of multi-patch B-spline meshes of blade cascades and their comparison. *Math. Comput. Simul.* **178**, 382–406 (2020).
- Mehrdada, N. S. et al. A novel optimization approach for axial turbine blade cascade via combination of a continuous-curvature parameterization method and genetic algorithm. *J. Mech. Sci. Technol.* **35**(9), 3989–4000 (2021).
- Moradtabrizi, H., Bagheri, E. & Nejat, A. Aerodynamic optimization of a 5 Megawatt wind turbine blade. *Energy Equip. Syst.* **2**(4), 133–145 (2016).
- Gribin, V. G. et al. A method for parametrically representing the aerodynamic profiles of axial turbine machinery blades. *Therm. Eng.* **67**(7), 422–429 (2020).
- Noori Rahim Abadi, S. M. A. et al. CFD-based shape optimization of steam turbine blade cascade in transonic two phase flows. *Appl. Therm. Eng.* **112**, 1575–1589 (2017).
- Kaviani, H. & Nejat, A. Aeroacoustic and aerodynamic optimization of a MW class HAWT using MOPSO algorithm. *Energy* **140**(1), 1198–1215 (2017).
- Selcuk, C. U. & Nathan, W. L. Turbomachinery design of an axial turbine for a direct fired sCO₂ cycle. *Energy Convers. Manage.* **267**, 1–15 (2022).
- Trigg, M. A., Tubby, G. R. & Sheard, A. G. Automatic genetic optimization approach to two-dimensional blade profile design for steam turbines. *J. Turbomach.* **121**(1), 11–17 (1997).
- Dennis, B. H., Dulikravich, G. S. & Han, Z. X. Optimization of turbomachinery airfoils with a genetic/ sequential quadratic programming algorithm. *J. Propul. Power* **17**(5), 1123–1128 (2015).
- Adjei, R. A., Wang, W. Z. & Liu, Y. Z. Aerodynamic design optimization of an axial flow compressor stator using parameterized free-form deformation. *J. Eng. Gas Turb. Power* **141**(10), 1010–1026 (2019).
- Couto, L. D. et al. Multi-objective structural optimization of a composite wind turbine blade considering natural frequencies of vibration and global stability. *Energies* **16**(3363), 1–25 (2023).
- Zhang, J. K. et al. Multi-objective optimization of aerodynamic and erosion resistance performances of a high-pressure turbine. *Energy* **277**, 1–14 (2023).
- Bonaiuti, D. On the coupling of inverse design and optimization techniques for the multi-objective, multipoint design of turbomachinery blades. *J. Turbomach.* **131**(2), 14–29 (2009).
- Park, J. & Sandberg, I. Approximation and radial-basis-function networks. *Neural Comput.* **5**(2), 305–316 (2014).
- Koch, P. N. et al. Statistical approximations for multidisciplinary design optimization: The problem of size. *J. Aircr.* **36**(1), 275–286 (2012).
- Simpson, T. W. et al. Kriging models for global approximation in simulation-based multidisciplinary design optimization. *AIAA J.* **39**(12), 2233–2241 (2015).
- Huang, Z. J. et al. Optimal design of aero engine turbine disc based on kriging surrogate models. *Comput. Struct.* **89**(1–2), 27–37 (2011).
- Bakhtiari, F. et al. Design and optimization of a new stator for the transonic compressor rig at TU darmstadt. *Am. Soc. Mech. Eng.* **93**(3), 595–598 (2015).
- Kadhim, H. T. & Rona, A. Design optimization workflow and performance analysis for contoured end walls of axial turbines. *Energy* **149**, 875–889 (2018).
- Chen, Y. R. et al. Surrogate models for twin-VAWT performance based on Kriging and artificial neural networks. *Ocean Eng.* **273**, 113947 (2023).
- Cardoso Netto, D., Ramirez Gustavo, R. & Manzanares Filho, N. Surrogate-based design optimization of a H-Darrieus wind turbine comparing classical response surface, artificial neural networks, and kriging. *J. Appl. Fluid Mech.* **16**(4), 703–716 (2023).
- Esfahanian, V. et al. Aerodynamic shape optimization of gas turbines: a deep learning surrogate model approach. *Struct. Multidisc. Optim.* **67**, 2 (2024).
- Wang, Z. F. et al. An optimization framework for wind farm layout design using CFD-based Kriging model. *Ocean Eng.* **293**, 116644 (2024).
- Badhurshah, R. et al. High efficiency design of an impulse turbine used in oscillating water column to harvest wave energy. *Renew. Energy* **121**, 344–354 (2018).
- Dykas, S., Włodzimierz, W. & Lukowicz, H. Prediction of losses in the flow through the last stage of low-pressure steam turbine. *Int. J. Numer. Meth. Fluids* **53**(6), 933–945 (2007).
- Dykas, S. et al. Experimental study of condensing steam flow in nozzles and linear blade cascade. *Int. J. Heat Mass Transf.* **80**, 50–57 (2015).
- Zhang, L. et al. Numerical analysis method for intra-stage non-equilibrium two-phase condensing flow in wet steam turbine and its application. *Int. J. Therm. Sci.* **193**, 1–11 (2023).
- Bhattacharyya, S. & Dutta, P. *Handbook of Research on Computational Intelligence for Engineering, Science, and Business* 479–500 (IGI Global, 2013).
- Ozkan, R. & Genc, M. S. Multi-objective structural optimization of a wind turbine blade using NSGA-II algorithm and FSI. *Aircr. Eng. Aerosp. Technol.* **93**(6), 1029–1042 (2021).

Acknowledgements

This work supported by the National Natural Science Foundation of China (No. 51609251).

Author contributions

L.Z.: Conceptualization, Methodology, Writing—Original Draft. G.C.: Data Curation, Formal Analysis, Visualization. Y.S.: Investigation, Validation, Writing—Review & Editing. L.X.: Investigation, Data Curation, Methodology. All authors reviewed and approved the final manuscript.

Funding

National Natural Science Foundation of China, 51609251, 51609251.

Declarations

Competing interests

The authors declare no competing interests.

Additional information

Correspondence and requests for materials should be addressed to L.Z. or Y.-A.S.

Reprints and permissions information is available at www.nature.com/reprints.

Publisher's note Springer Nature remains neutral with regard to jurisdictional claims in published maps and institutional affiliations.

Open Access This article is licensed under a Creative Commons Attribution-NonCommercial-NoDerivatives 4.0 International License, which permits any non-commercial use, sharing, distribution and reproduction in any medium or format, as long as you give appropriate credit to the original author(s) and the source, provide a link to the Creative Commons licence, and indicate if you modified the licensed material. You do not have permission under this licence to share adapted material derived from this article or parts of it. The images or other third party material in this article are included in the article's Creative Commons licence, unless indicated otherwise in a credit line to the material. If material is not included in the article's Creative Commons licence and your intended use is not permitted by statutory regulation or exceeds the permitted use, you will need to obtain permission directly from the copyright holder. To view a copy of this licence, visit <http://creativecommons.org/licenses/by-nc-nd/4.0/>.

© The Author(s) 2025